MOLECULAR SIMULATION
2020, VOL. 46, NO. 3, 224–234
https://doi.org/10.1080/08927022.2019.1690145

Taylor & Francis
Taylor & Francis Group

Wetting of single crystalline and amorphous silicon surfaces: effective range of intermolecular forces for wetting

H. Gokberk Ozcelik[a], A. Cihan Ozdemir[a], Bohung Kim[b] and Murat Barisik [a]

[a]Department of Mechanical Engineering, Izmir Institute of Technology, Izmir, Turkey; [b]School of Mechanical Engineering, University of Ulsan, Ulsan, South Korea

ABSTRACT

Wetting at nanoscale is a property of a three-dimensional region with a finite length into the solid domain from the surface. Understanding the extent of the solid region effective on wetting is important for recent coating applications as well as for both crystalline and amorphous solids of different atomic ordering. For such a case, we studied the wetting behaviour of silicon surfaces at various crystalline and amorphous states. Molecular distributions of amorphous systems were varied by changing the amorphisation conditions of silicon. Semi-cylindrical water droplets were formed on the surfaces to be large enough to remain independent of line tension and Tolman length effects. Contact angles showed up to 38% variation by the change in the atomic orientation of silicon. Instead of a homogeneous solid density definition, we calculated different solid densities for a given surface measured inside different extents from the interface. We correlated the observed wetting variation with each of these different solid densities to determine which extent governs the wetting variation. We observed that the variation of solid density measured inside a 0.13 nm extent from the surface reflected the variation of wetting angle better for both single crystalline and amorphous silicon surfaces.

ARTICLE HISTORY
Received 1 April 2019
Accepted 18 October 2019

KEYWORDS
Surface wetting; single crystalline and amorphous silicon; molecular dynamics

The wetting behaviour of solids is significant for a wide range of applications. From macro to nanoscale, wetting highly influences ice/fog formations on a surface, fluid transport inside a channel/tube and heat conduction from a surface to a fluid. Hence, being able to manipulate wetting can control those mechanisms. One of the most common methods to design the wetting is surface coatings. With advances in nanotechnology, two-dimensional materials and thin films have been utilised to cover a given surface with a different material of desired wetting at nanometre scales. However, discrepancies regarding the physics related to nanoscale wetting behaviour remain.

The influence of coating on wetting differs from case to case. For example, one of the most popular two-dimensional materials, graphene, was presented as a coating which is transparent to wetting properties of the underlying surface [1]. Such behaviour can be useful for heat transfer applications. For instance, a hydrophilic material with high interface heat conductance can remain hydrophilic but become protected from possible corrosive effects [2]. This wetting transparency develops for hydrophobic atomistically smooth one atom thick monolayer graphene which exerts weak molecular forces onto water but allows the intermolecular forces from the underneath substrate to remain effective. On the other hand, the same monolayer graphene is found partially wetting transparent in case of superhydrophobic and superhydrophilic surfaces [3] or non-transparent for surfaces whose wetting is mostly dominated by chemical bonding between water and substrate, such as glass [4]. Such physics show that wetting is a resultant of intermolecular force interactions of a group of molecules in a three-dimensional region with a finite extent in the surface normal direction. Similar behaviour was also observed for other two-dimensional materials such as molybdenum disulphide [5], tungsten disulphide [6], hafnium dioxide [7] and phosphorene [8]. With the increase of coating layers, surface wetting reaches to wetting characteristic of the coating material. Hence, in the case of nanoscale coatings, adjacent liquid interacts with underneath substrate at various extents for transparent, partially transparent (translucent) and weakly transparent coating conditions.

Multiple studies have been dedicated to investigating the novel wetting physic observed at nanoscale. For example, graphene-coated hydrophobic and hydrophilic surfaces may be engineered to develop the same contact angle, by tuning the corresponding molecular properties [9]. As the solid/liquid interfacial coupling is a function of inter/intramolecular interactions, a better understanding of the region extending a couple of nanometres from the interface is required to manipulate the wetting dominated by dispersive or polar forces. Ramos-Alvarado et al. proved that the atomic sequence strongly influence the wetting [10]; silicon surfaces at different crystal planes result in different contact angles due to the varying density of surface atoms (contact angles of $87.7° \pm 0.36°$ and $103.6° \pm 0.45°$ were obtained for Si(111) and Si(100), respectively). Variation of wetting by variation in the surface crystal plane was observed in many other materials as well [11–13]. Researchers tried to theoretically describe the influence of solid molecular density on Van der Waals interactions [3,10,14,15]. They emphasised that the contact angle can be predicted by an accurate quantification of both solid and liquid densities at and near

CONTACT Bohung Kim bohungk@ulsan.ac.kr, Murat Barisik muratbarisik@iyte.edu.tr

the interface region. However, the influence of solid density was analysed using a homogeneous volumetric density definition calculated by assuming a semi-infinite solid. Such characterisation neglects the atomic distribution of a given crystal structure, and is unable to ultimately describe the wetting angle variation by the crystal structure since the average homogenous density of a solid is constant independent of molecular distribution. As the great deal of 'wetting transparency' studies also suggested, the contribution of solid molecules onto overall wetting behaviour shows variation by their atomic location in a three-dimensional space. The extent of dispersive interactions between liquid and substrate and the corresponding effective solid atoms near the interface need to be quantified for a proper description of the effective wetting region inside the solid and the corresponding solid surface molecular density governing the wetting.

The crystal structure of silicon is a diamond cubic lattice which yields a large number of different crystal planes depending on the angle of cut in manufacturing processes. Varying the angle of the cut from 0° to 54.7°, crystal plane will change from (001) to (111) while in between, there are 14 additional other crystal planes with different unit cell sizes [16]. Different crystal planes result in the different molecular structure on the surface. Surface structures can also be further changed through various processes such as relaxation or reconstruction. There are various techniques to produce perfectly single crystalline silicon, but many techniques yield poly-crystalline surfaces which will develop local molecular structure variation on the surface. Overall, manipulating the surface crystal plane can control the surface molecular structure and resulting interface properties. Engineering wise, it is much simpler to produce amorphous silicon structures, instead of ordered crystalline ones. Different solidification techniques create different molecular distributions. Specifically, it was presented that the solidification cooling rate [17–19] and pressure [20–23] can control the molecular density at the interface regions. Such mechanisms can be used to manipulate the surface wetting; however, its possible influence on surface wetting has not been characterised yet in the literature.

In the characterisation of nanoscale wetting, the size dependence of a contact angle has been presented by both experiments [24,25] and molecular level simulations [26,27]. Basically, two major mechanisms affect the wetting behaviour at nanoscale and yield deviations from the classical description of Young's equation. As the droplet size decreases, (i) the 'line tension' along the three-phase contact line becomes increasingly important [28] while (ii) the liquid–vapour interface surface tension changes as a function of curvature and 'Tolman length' [29]. Current literature modified Young's equation to include line tension [30] and Tolman correction [31] as a function of the radius of three-phase line (r_B) and radius of droplet (R) as

$$\gamma_{SV_\infty} = \gamma_{SL_\infty} + \gamma_{LV_\infty}\left(1 - 2\frac{\delta}{R}\right)\cos\theta + \frac{\tau}{r_B}, \tag{1}$$

where $\gamma_{SV\infty}$, $\gamma_{SL\infty}$ and $\gamma_{LV\infty}$ are the interfacial tensions at the boundaries between liquid (L), solid (S) and vapour (V) at macroscopic scales (∞), δ is the Tolman length, τ is the line tension between the droplet and surface and θ is microscopic contact angle. Microscopic contact angle, θ, can be defined in terms of the macroscopic contact angle as

$$\cos\theta_\infty = \left(1 - 2\frac{\delta}{R}\right)\cos\theta + \frac{\tau}{r_B\gamma_{LV_\infty}}, \tag{2}$$

which can be simplified into

$$\frac{(R-2\delta)\gamma_{LV_\infty}\sin 2\theta + 2\tau}{\sin\theta} = 2R\gamma_{LV_\infty}\cos\theta_\infty. \tag{3}$$

Equation (3) estimates the contact angle of a nanoscale spherical droplet as a function of the droplet radius. However, corresponding Tolman length and line tension values are controversial. Multiple Molecular Dynamics (MD) studies were dedicated to investigating size dependent behaviour in nanoscale wetting [32,33]. It is also a common practice for MD studies to simulate large enough cylindrical water droplets to obtain negligible curvature at the liquid–vapour interface and zero curvature at a three-phase line [34,35] in order to eliminate the Tolman and line tension effects from their measurements. Reported Tolman length values vary around ~0.05 nm for water–vapour interface [36,37]. In addition to these two nanoscale effects, a pining force onto three-phase contact line develops in the case of a nanoscale chemical [38] or physical surface heterogeneity [39], which may keep the liquid front at a metastable state and create a wetting angle significantly different than its equilibrium value [40]. Further modification of Young's equation was proposed for nano-structured surfaces to consider 'pinning effect' on the droplet contact line [41].

The objective of this study is to investigate the effect of an interface region's molecular structure and sequence on surface wetting. To accomplish this, various forms of single crystalline and amorphous silicon surfaces will be studied by Molecular Dynamics simulations (MD). Semi-cylindrical water nano-droplets will be used in contact angle calculations in order to eliminate the three-phase line tension effects. Using different amorphisation pressures, near interface solid structures will be varied in a controlled manner. Solid and liquid density profiles and the corresponding contact angles will be correlated to characterise the region effective on wetting. Surface atomic densities will be defined and measured at different extents from the interface in order to describe the contact angles.

1. MD simulation details

Large-scale Atomic/Molecular Massively Parallel Simulator (LAMMPS) Code [42] is used as an MD solver. The simulation domain is formed by a silicon slab and a nanoscale water droplet. Silicon at different crystal planes has different lattice constants. For such a case, simulation boxes were formed approximately 15 nm × 5 nm × 10 nm dimensions in $x \times y \times z$-directions, respectively. A periodic boundary condition was imposed on x and y direction while the z-direction was bounded with a specular reflection boundary. A large group of possible silicon surfaces were molecularly created, and their near surface densities were measured. Since some of these surface planes created very similar surface densities, we

selected only six single crystalline structures to represent a range in variation of surface molecule density. Specifically, (110), (111), (001), (112), (120) and (021) planes were chosen. We produced amorphous silicon structures by melting and then cooling the silicon at a constant volume and constant temperature conditions of the NVT ensemble. Starting from the (111) plane configuration with approximately 7000 atoms, silicon structure annealed to 2000 K to obtain a melt by applying NVT ensemble for 2 ns and later NVE ensemble for another 2 ns for a complete equilibrium at 2000 K. After reaching equilibrium, liquid silicones were quenched to 300 K at the rate of 10^{12} Ks^{-1}. We kept the cooling rate constant at 10^{12} Ks^{-1} which was validated to develop experimental measured amorphous silicon structure [43]. On the other hand, we varied the volume of simulation domain in the surface normal direction in order to vary molecular structure, similar to Titanium aluminide [19]. Our silicon slab was extending periodically in two directions while the third direction was the surface. Hence, we varied the height of confinement for melting and solidification processes, which created different melt densities. Different molecular distributions in amorphous silicon structures were obtained this way. Six different amorphous silicon structures were formed as a_1-Si, a_2-Si, a_3-Si, a_4-Si, a_5-Si and a_6-Si. We employed three body Tersoff potential [44], which was used by others to create amorphous silicon structures [45–47].

We formed 1728 water molecules placed on the silicon surface so water could form a hemi-cylindrical droplet on the surface. Semi-cylindrical water nano-droplets were used to eliminate the three-phase line tension effects [35]. Different water models were proposed as a fit to different physical properties of water but showed that repulsive part of dispersive forces and short-range electrostatic interactions are essential in capturing thermodynamic properties of water [48]. In the current simulations, SPC/E water model was employed for simplicity and computational cost. OH bond length of 0.1 nm and H–O–H angle of 109.47° were constrained with the SHAKE algorithm [49]. The interaction of hydrogen atoms was neglected. Partial charges q (0.4238 e) and −2q (−0.8476 e) were assigned each hydrogen and oxygen atom, respectively. A 1 nm cut off distance was defined for both Van der Waals and Coulombic interactions between water molecules while particle–particle particle–mesh (PPPM) solver is used to evaluate long-range Coulombic forces among water molecules. Van der Waals interactions are modelled with Lennard–Jones (L–J) potential given as

$$\Phi(r_{ij}) = 4\varepsilon\left(\left(\frac{\sigma}{r_{ij}}\right)^{12} - \left(\frac{\sigma}{r_{ij}}\right)^{6}\right), \quad (5)$$

where r_{ij} is the intermolecular distance, ε is the depth of the potential well, σ is the molecular diameter. The interaction parameters for similar molecular pairs used in the simulations are given in Table 1. It is a common practice to estimate the interaction parameters between dissimilar molecules using various forms of mixing rules. For example, for the silicone-oxygen interactions, parameters can be calculated by the Lorentz–Berthelot (L–B) mixing rule given as

$$\sigma_{Si-O} = \frac{\sigma_{Si-Si} + \sigma_{O-O}}{2}, \ \varepsilon_{Si-O} = \sqrt{\varepsilon_{Si-Si} \times \varepsilon_{O-O}}. \quad (6)$$

Using the corresponding parameters given in Table 1, the L–B mixing rule predicts the interaction parameters σ_{Si-O} = 2.6305 Å and ε_{Si-O} = 0.12088 eV. However, our earlier wetting study based on MD measured contact angles of water nano-droplets showed that experimentally measured hydrophobic behaviour of silicon surfaces can be recovered when the silicon-oxygen interaction strength is 12.5% of the value predicted using the Lorentz–Berthelot mixing rule [50]. For such a case, we employed our earlier proposed interaction strength value as ε_{Si-O} = 0.01511 eV.

The Verlet algorithm was applied to integrate Newton's equation of motion with a time step of 0.001 ps. The bottom layer of the silicon substrate was excluded from time integration to prevent the shift of silicon substrate. At the beginning of wetting simulations, Maxwell–Boltzmann velocity distribution was assigned for all molecules at 300 K. NVT ensemble with Nosé–Hoover thermostat was applied to keep the temperature at 300 K. Simulations were carried out 2×10^6 timesteps (2 ns) to reach an isothermal steady state. After that, microcanonical ensemble was employed to obtain averaging of the desired properties for 6×10^6 timesteps (6 ns). Averaging is performed with 5 ps intervals. Two different binnings were used for averaging. Due to the hemi-cylindrical droplet shape, long rectangular prisms with the size of 0.1 nm × ∞ × 0.1 nm along x, y and z directions were used to resolve droplets. On the other hand, slab bins with ∞ × ∞ × 0.01 nm along x, y and z directions were used to resolve the silicon domain.

Water density was averaged by bins in rectangular prism shape in the xz plane. Two-dimensional (2D) density contours which represent equally dense regions were extracted from bin-wise water distribution as shown in Figure 1(c). Molecular surface surfaces create density layering near surface that structure of the 2D density contours were found to be circular except in this near wall region. Contact angles were measured from these averaged density contours. First, the droplet boundary was determined as the points at which the density is half of bulk water (0.5 g/cm^3). Second, we fit a circle passing through the points 0.8 nm above the surface. Near wall, density points closer to the surface than 0.8 nm were omitted to avoid the influence from density fluctuations at the liquid–solid interface. Finally, the radius of the circle was denoted as r_{Droplet} while r_{Base} was defined at which circle meets the solid substrate. Using these, contact angles were geometrically calculated.

Table 1. Molecular interaction parameters utilised.

Molecule pair	σ (Å)	ε (eV)	q (e)
O–O	3.166	0.006739	−0.8476
H–H	0	0	+0.4238
Si–O	2.633	0.01511	0

2. Results and discussion

Cylindrical water droplets successfully formed on the selected single crystalline surfaces as given in Figure 1(a). These droplets extend through the periodic boundary. Different than the

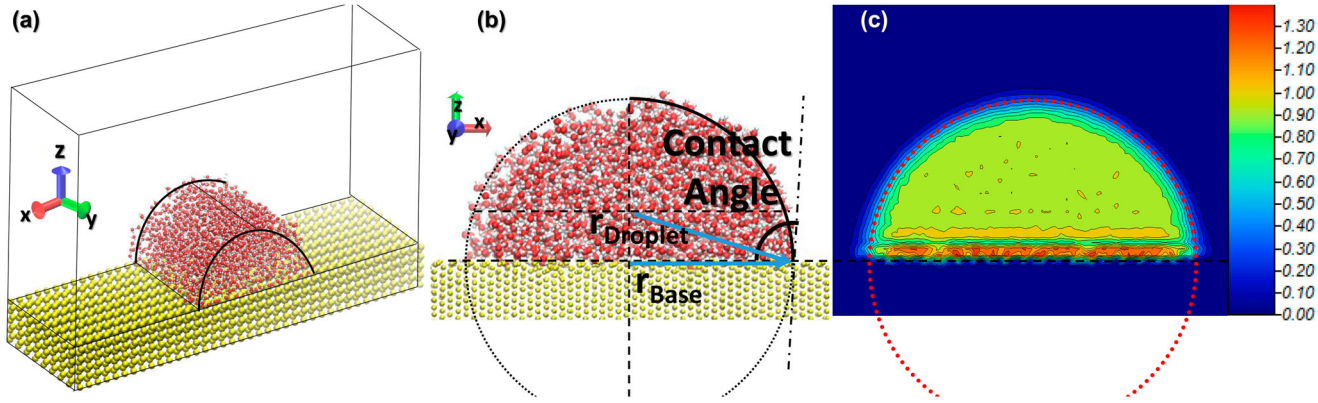

Figure 1. (Colour online) (a) The snapshot of simulation domain consisting of slabs and hemi-cylindrical water nano-droplet. (b) Schematic for the measurement of contact angle with the snapshot. Oxygen, hydrogen and silicon molecules are illustrated as red, white and yellow spheres, respectively. (c) Density contours in the *x*–*z* plane of the same case.

spherical droplets developing size dependent line tension effects, cylindrical droplet's liquid surface does not develop any curvature related line tension since the three-phase line is linear. Using current semi-cylindrical droplets, the wetting angle of surface can be obtained regardless of nano-droplet size.

Contact angles were measured as 80.2°, 88.4°, 101.4°, 84.4°, 89.3° and 92.8° at (110), (111), (001), (112), (120) and (021) planes, respectively (Figure 2). Observed differences on the contact angles are due to differences in solid molecular distribution. Even though water molecules and silicon atoms are interacting at a constant pair-wise molecular potential, the configuration of silicon atoms at near interface region, such as orientation and density, resulted in almost 25% variation in wetting angle in these single crystalline surfaces.

Although cylindrical droplet shape prevents line tension effects, liquid surface tension could be still developing a size dependent behaviour due to Tolman's length. Hence, we simulated different size cylindrical droplets and measured contact angles. Figure 3 presents the wetting behaviour of cylindrical droplets with base radius varying between 7.2 nm (Figure 3(a)) and 3.5 nm (Figure 3(g)) on the (112) silicon surface. Wetting angle remained almost identical in the studied droplet range showing that the Tolman length is small and has a negligible effect on the current system. Although the studied surfaces are smooth, there is an atomic roughness that is necessary to investigate any possible pinning effects. For this purpose, we picked the (112) surface showing the highest atomic corrugation. However, as the contact angles remained independent of droplet size in Figure 3, the pinning effect does not affect the current wetting measurements.

Next, local molecular variation in surface normal direction was studied in terms of densities measured in one-dimensional slab bins. Number density of silicon and mass density of water are given in Figure 4. Results of the different cases are plotted at similar extents in surface normal direction while zero point of height was simply defined as the location where solid density becomes zero. The well-known liquid density layering was observed in water densities on the silicon surface [][51].

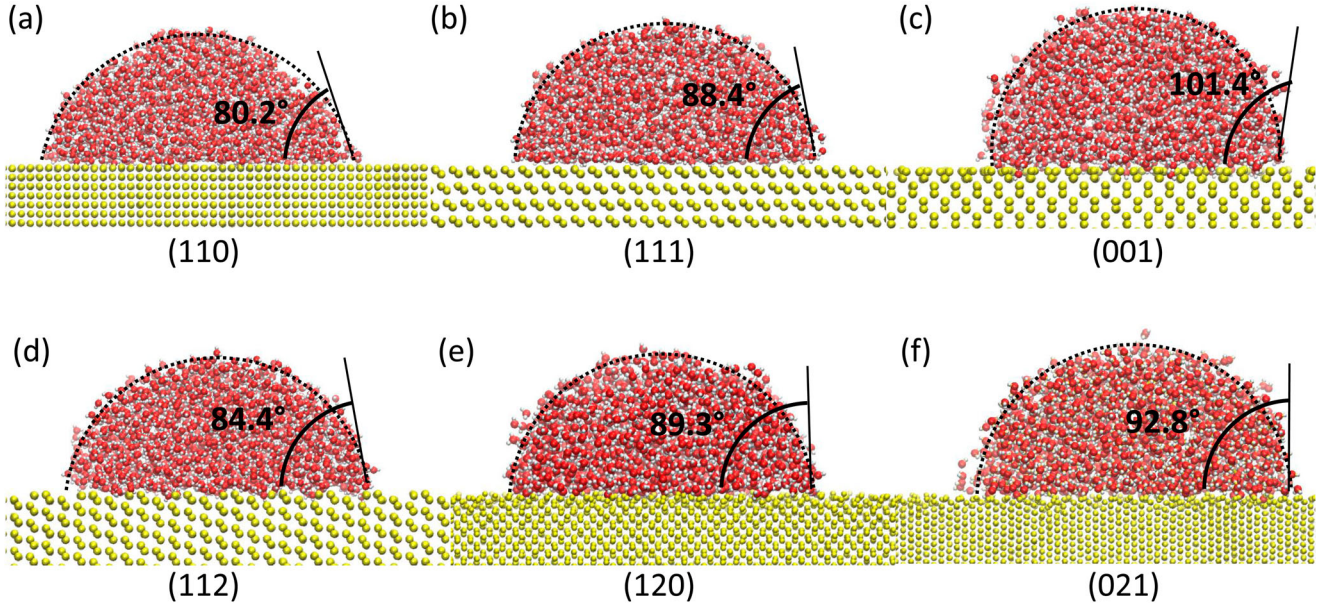

Figure 2. (Colour online) Contact angles of single crystalline silicon with (a) (110), (b) (111), (c) (001), (d) (112), (e) (120) and (f) (021) crystal planes at the surface.

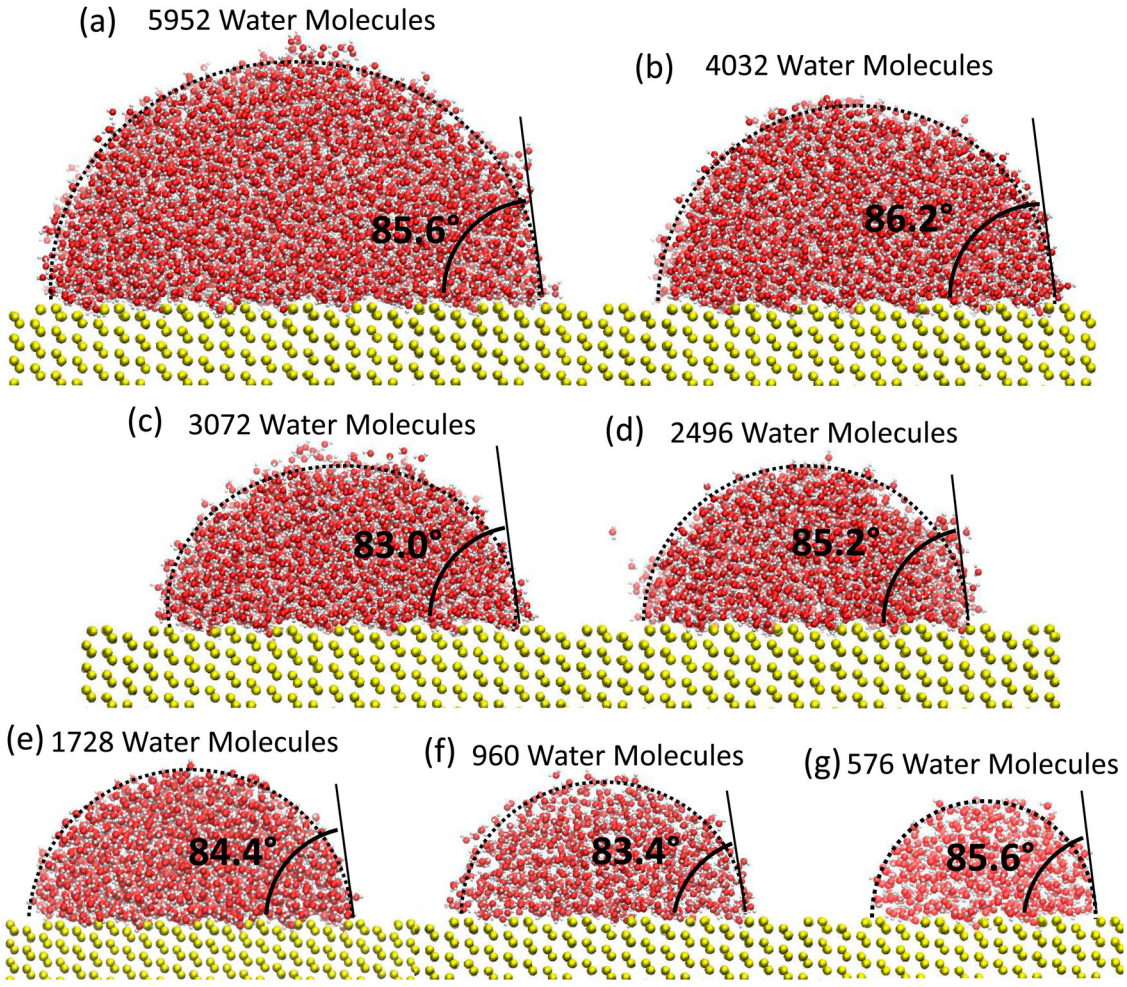

Figure 3. (Colour online) Wetting angles measured by different size water droplets containing (a) 5952, (b) 4032 (c) 3072, (d) 2496, (e) 1728, (f) 960 and (g) 576 number of water molecules on (112) surface.

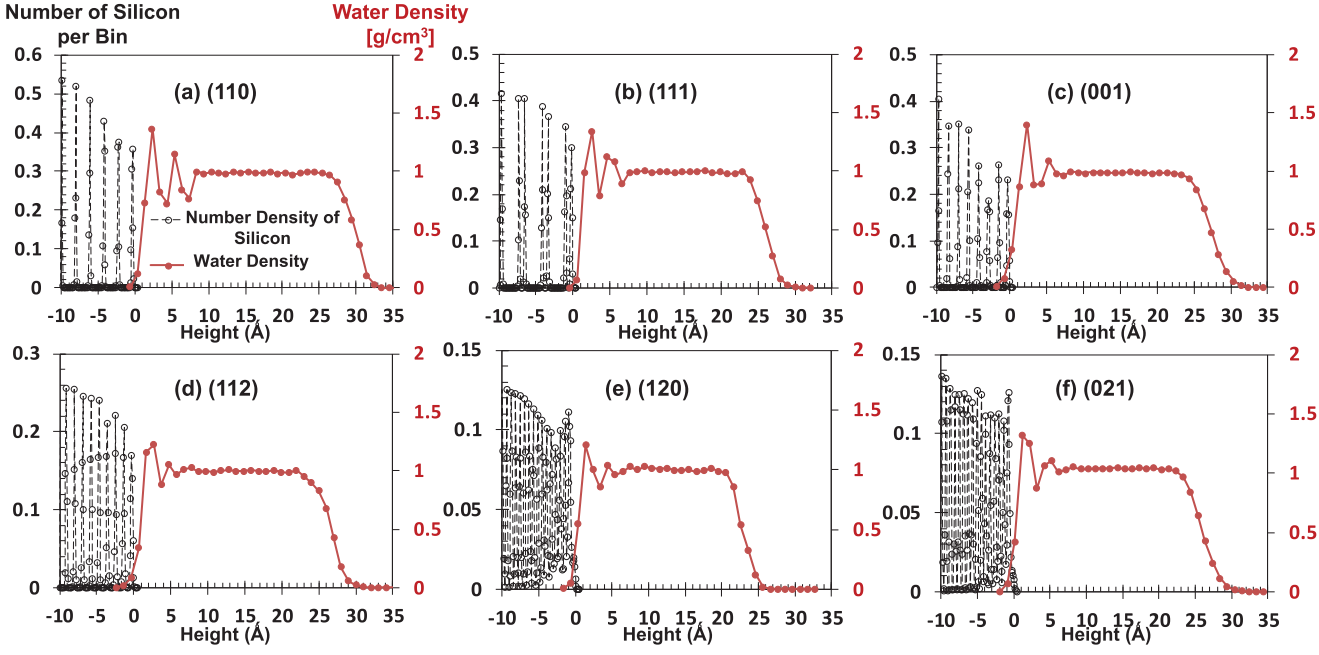

Figure 4. (Colour online) Bin-wise density distribution of silicon and water. Silicon densities are presented in the left axis and water densities are presented in the right axis.

Water density reaches its thermodynamically defined value of 1 g/cm^3 at the bulk, sufficiently away from the surface. Higher first density peaks observed in Figure 4(a–c) than those in Figure 4(d–f). When the wetting angle of silicon structures are taken into account, higher contact angle results in, relatively, lower density peaks. A similar trend was also seen in the study [50] which supports the discussion that the contact angle is associated with the first fluid layer [52]. On the solid side of the interface, wider solid molecule ordering develops higher bin-wise silicon number densities separated with empty bins. On the other hand, more uniform solid ordering results in lower bin-wise number density and lower empty bins in between. Overall averaging of bin-wise densities yields the thermodynamic density of silicon as 2.33 g/cm^3, very close to experimentally measured values [53]. Figure 4 shows that layering of water molecules near the surface is directly related to the silicon number density as the higher density peaks of water molecules are observed in higher density spikes of silicon or vice versa.

The objective was to develop and study a very similar interface mechanism for amorphous silicon. We built amorphous silicon blocks at a constant cooling rate, but at different melt densities varied by the amorphisation volume, as described in the earlier 'Simulation Details' section. Simulation boundary in the surface normal direction is slightly changed during the melting and cooling process that the amorphous silicon density at 300 K remained the same at every case while molecular distributions developed variation. In Figure 4, six different amorphous silicon structures and contact angles measured are presented. Contact angles of amorphous silicon blocks varied between 82.1° and 109.7° while amorphisation height was increased (Figure 5(a–f)). Although there is an outlier, Figure 5 shows that the increase of amorphisation volume yields up to 38% increase in contact angle.

Similar to earlier investigations, possible size dependence of measured contact angles was investigated for the amorphous silica surface. Figure 6 presents wetting angles of cylindrical water droplets with varying base radius. Very similar contact angles were measured which shows that the Tolman length and pining effect have negligible effects on the current system.

We further investigated the adsorption behaviour by measuring the interaction potential between one water molecule and each of the amorphous surfaces. We determined 11 locations on the surface under the cylindrical droplet as described in Figure 7(a). Interaction potentials of indentation of a water molecule at each location are given in Figure 7(b,c) over the a_1-Si and a_4-Si surfaces. The potential distributions vary due to the atomic corrugation on the surface. The potential wells of different sites over a_1-Si surface are located very close while the potential wells over a_4-Si distributed in a wider area as a result of increased atomic roughness. Figure 7 (c) compares the average potential distributions of each amorphous surface. Even though the depth of the average potential wells of different surfaces are very similar, the location of potential wells is pushed away from the surface by the increase of amorphisation height. This simply suggests that the surface repeals water.

To better understand the observed wetting dynamics, we studied the density profiles of both silicon and water in the surface normal direction in Figure 8. Since the amorphous silicon molecules are randomly distributed, a less fluctuating bin-wise silicon density distribution was measured. Bulk silicon density of all six different cases are at 2.33 g/cm^3, which is a well-accepted density for amorphous silicon [43]. On the other hand, density at near interface decreases with increasing amorphisation height, which was also observed by others [20,21]. In the densest case, density at the interface reaches to double the bulk density as shown in Figure 8(a). Water density layering

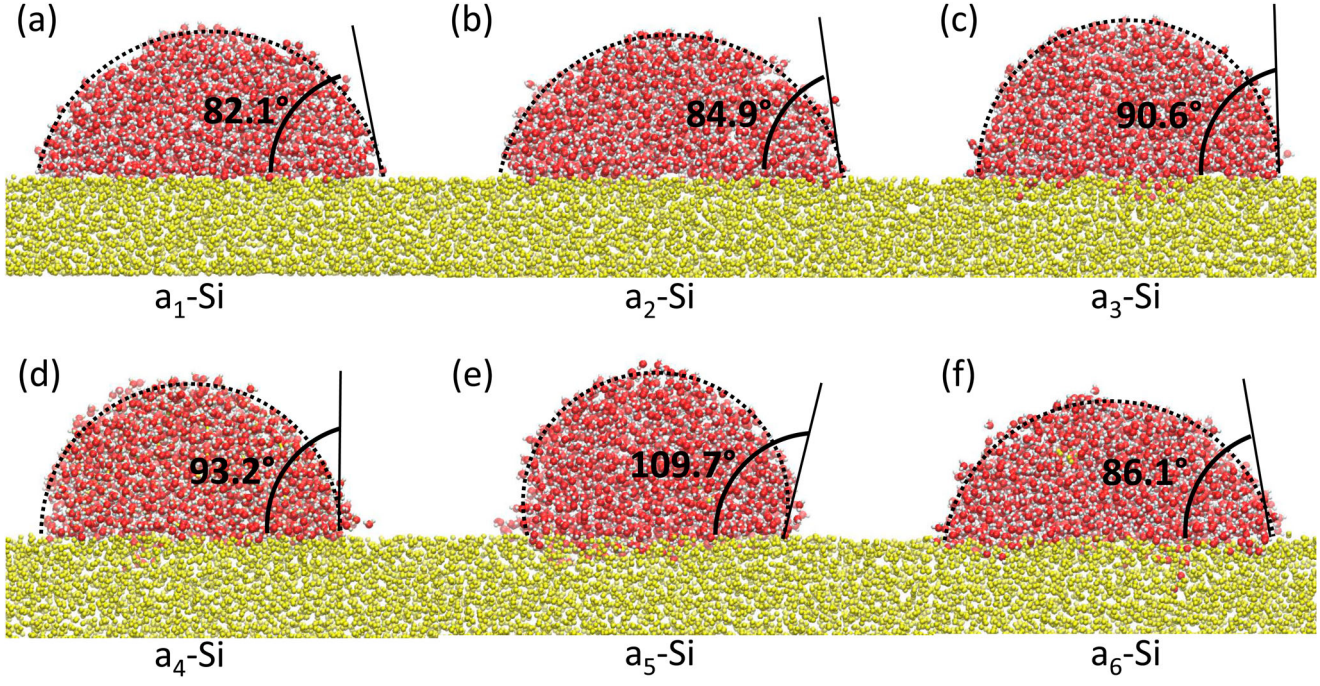

Figure 5. (Colour online) Six different amorphous silicon structures of (a) a_1-Si, (b) a_2-Si, (c) a_3-Si, (d) a_4-Si, (e) a_5-Si and (f) a_6-Si with corresponding wetting angles.

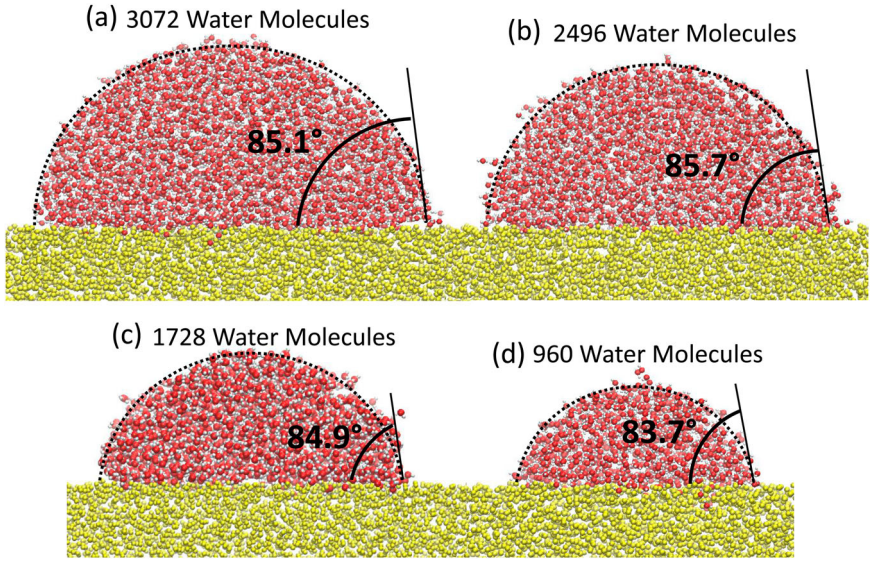

Figure 6. (Colour online) Wetting angles measured by different size water droplets containing (a) 3072, (b) 2496, (c) 1728 and (d) 960 number of water molecules on a_2-Si surface.

responses to this variation in molecular structuring such as the highest density layering of water molecules is observed on the densest near silicon case. Furthermore, a decreased density of silicon molecules allows water molecules to diffuse into silicon slab and in the least dense case, small density peaks of water molecules are seen inside amorphous silicon substrate as shown in Figure 8(f). Moreover, diffusion of an excessive amount of water into silicon substrate changes the wetting

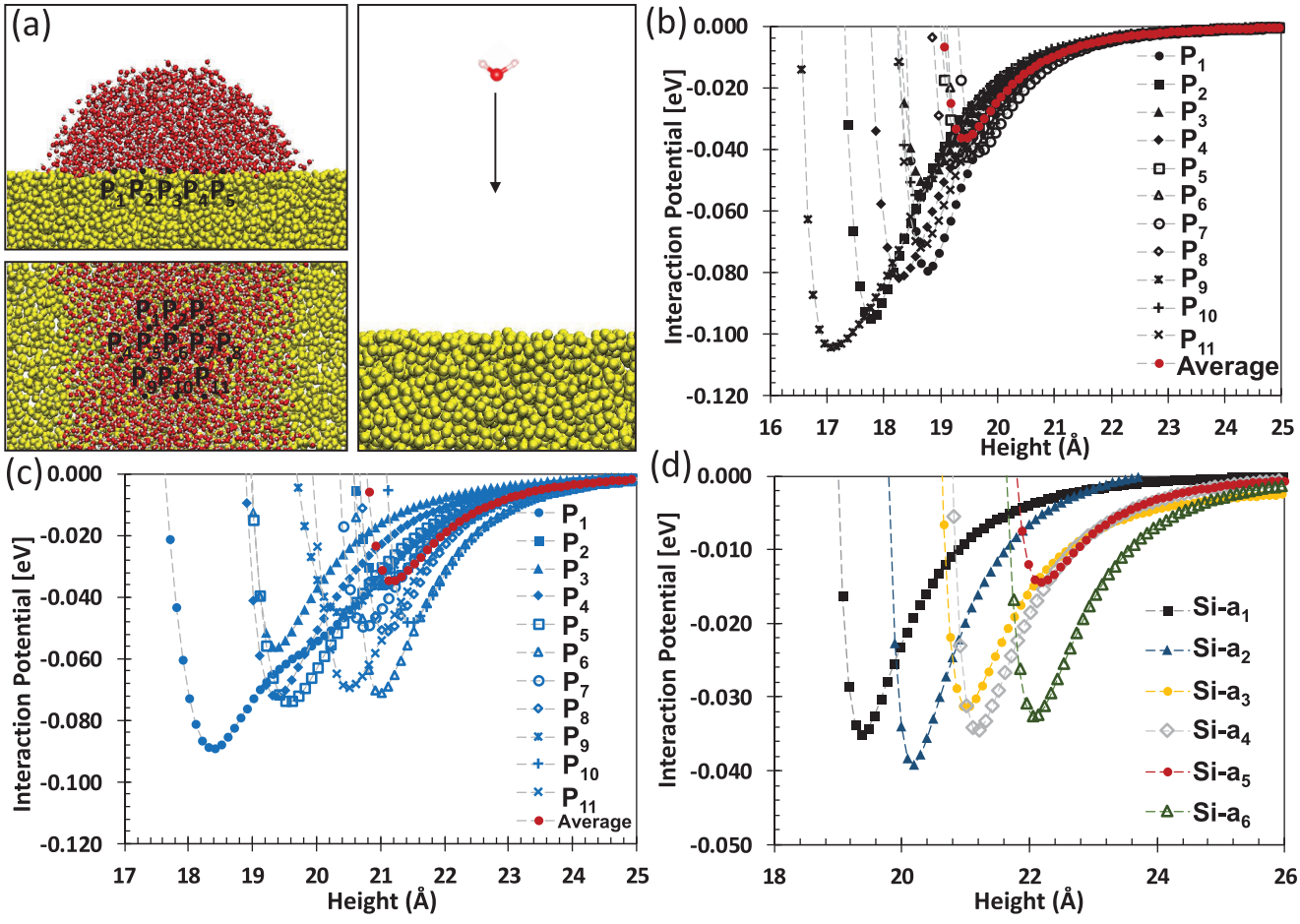

Figure 7. (Colour online) (a) Surface locations under the cylindrical droplet selected for indentation. Interaction potential measured at each location over (b) a_1-Si and (c) a_4-Si surfaces. (d) Comparison of average interaction potentials measured on different amorphous surfaces.

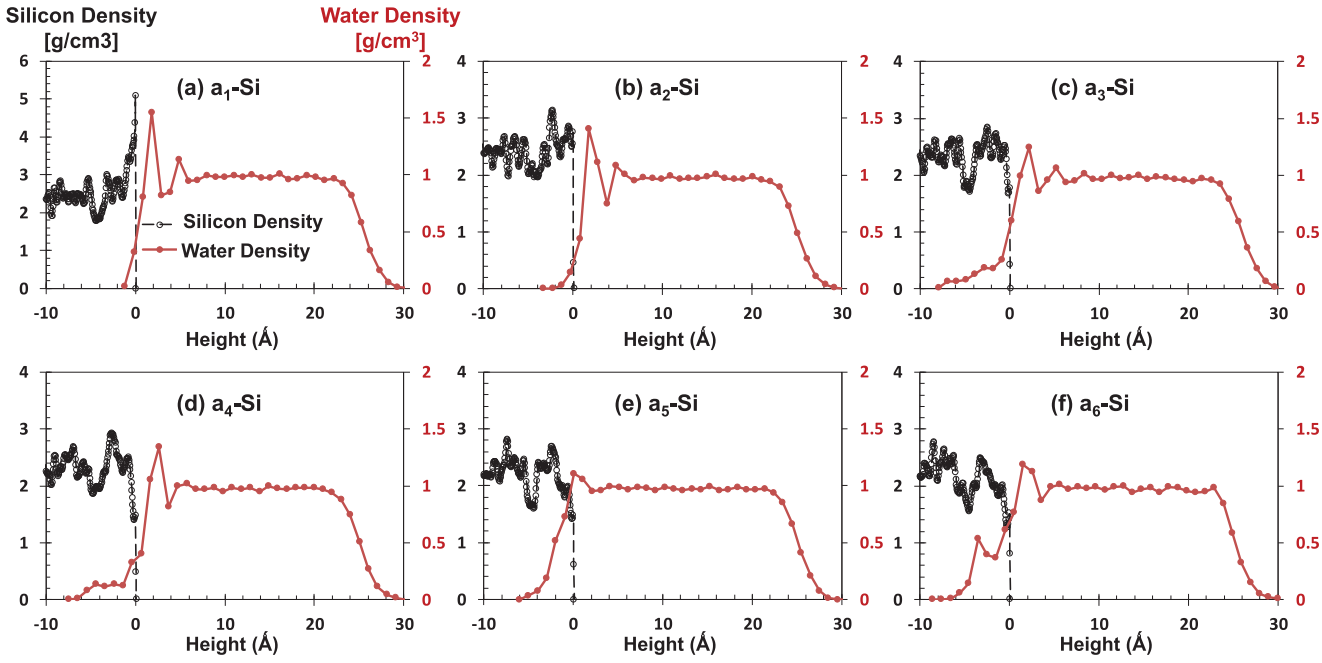

Figure 8. (Colour online) Bin-wise density distribution of amorphous silicon and water. Silicon densities are presented in the left axis and water densities are presented in the right axis.

dynamics that wetting angle of a-si$_6$ surface diverges from the trend (Figure 5).

The atomistic structure and resulted in the oscillatory density profile of amorphous silicon are similar to experimental measurements [54]. The molecular orders of different amorphous structures in this 1 nm thick solid region are similar to each other, except very near interface region. So, the molecular structure near the interface must be responsible for the variation of the wetting angle. For a better characterisation, we sought to define a near interface solid density. We specified a near interface height parameter (h) as the distance from the interface towards the amorphous silicon structure, as illustrated in Figure 9(a). We measured solid density at different h values of $h = 0.13$, 0.26 and 0.39 nm while the h greater than 0.5 nm yield to bulk silicon density. Figure 9(b) presents amorphous silicon near interface densities measured by covering different heights of the interface region, compared with the bulk density measured, for all six different amorphous structures. The average bulk densities show negligibly variation for different amorphous silicon structures, but near the surface, densities show strong variation for different amorphous structures. Two major behaviours were observed. First, near interface densities decrease by increasing amorphisation height. Second, with an increase in interface region height, interface density reaches to bulk density value by either increasing or decreasing, depending on the amorphous surface. This means interface density is higher than bulk in some cases (a$_1$-Si, a$_2$-Si and a$_3$-Si) but lower at others (a$_4$-Si, a$_5$-Si and a$_6$-Si).

Near interface densities inside different interface, heights were also calculated for the studied single crystalline systems. Using this data, we tried to correlate interface solid density with the wetting angles measured on the corresponding

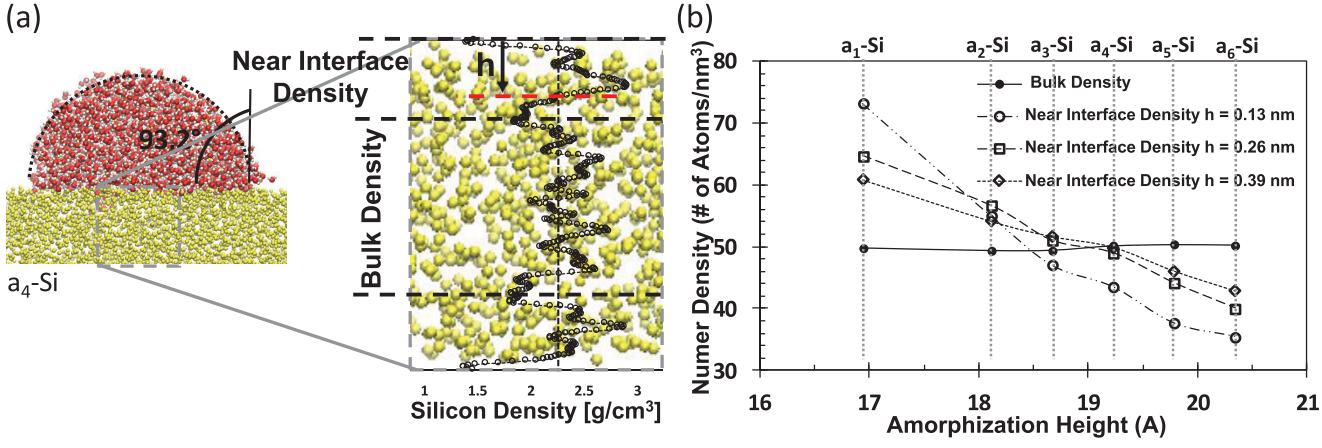

Figure 9. (Colour online) (a) Illustration of the near interface density and near interface height definitions. (b) Near interface densities measured at different interface heights for the studied six amorphous structures developed at different amorphisation heights.

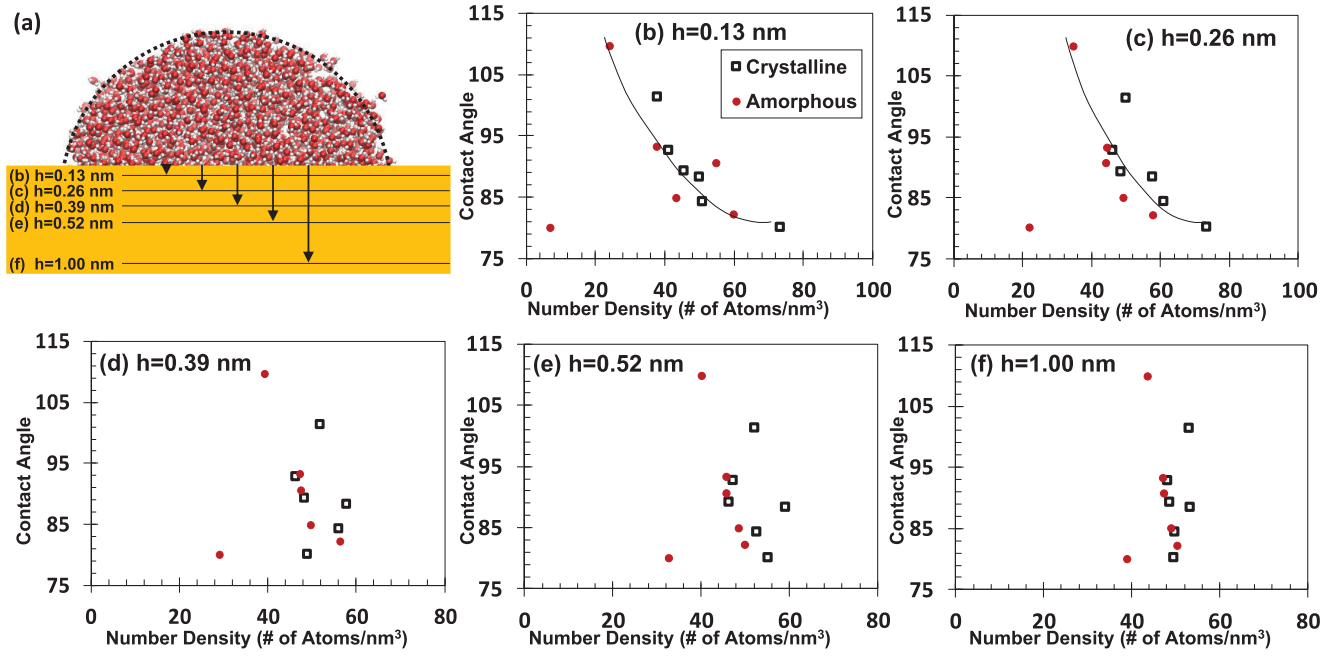

Figure 10. (Colour online) (a) Illustration of near interface regions where solid surface densities were calculated. (b)–(f) Contact angles on different single crystalline and amorphous surfaces as a function of densities measured inside different near interface heights (*h*).

cases in Figure 10. Simply, we plotted the variation of contact angle as a function of interface number density measured inside interface regions extending 0.13, 0.26, 0.39, 0.52 and 1 nm from the interface. The schematic representation of the near interface region is given in Figure 10(a). All contact angles measured on both single crystalline and amorphous silicon as a function of number density are plotted in Figure 10 (b–f) for different near interface regions created by different *h* values. First, the wider interface regions extending 1, 0.52 and even 0.39 nm yielded to calculate very similar density values in these different cases. Such an occurrence cannot be explained by the variation of contact angle, as seen in Figure 10(d–f). On the other hand, densities measured inside interface regions extending both 0.13 and 0.26 nm developed different density values at different cases. For such a case, Figure 10(b,c) presents that the wetting angle decreases with an increase in interface density. Specifically, contact angle variation described best by variation of density in $h = 0.13$ nm region in Figure 10 (b). Hence, wetting behaviour is mostly governed by the solid molecules one (0.13 nm) or at most two (0.26 nm) molecular diameter away from the interface.

3. Conclusion

Advance manufacturing technologies can produce atomistically smooth surfaces at a desired molecular structure or sequence. In the corresponding applications, surface energies and resulting interface coupling between solids and fluids at nanoscale play key roles. Nanoscale wetting differs from the continuum surface wetting definition; instead of being a two-dimensional surface property, nanoscale wetting is governed by the interaction from a finite three-dimensional region whose extent in the surface normal direction is non-negligible. Such a perspective is widely utilised by the most recent surface engineering applications using thin films and two-dimensional materials. For example, wetting transparency introduced for various thin coating materials is based on the idea that wetting is not greatly affected by the very near interface material but dominated by the underneath solid molecules in a three-dimensional span from the interface. There have been multiple studies dedicated to test this idea, but there is no conclusion about the extent of the region governing the wetting behaviour. Also, solid atomic distribution on/under surface is found affecting the wetting of atomistically smooth simple materials. Parallel to these, researchers proposed analytical models which can predict wetting angle as a function of the density of solid surface and near liquid. However, these mostly focused on the interface liquid density by assuming a homogeneous solid density. In order to provide a fundamental knowledge, we simplified this query to the uniform silicon systems, instead of developing case specific results for different levels of atomic heterogeneities by coatings.

We studied the wetting behaviour on the single crystalline and amorphous silicon surfaces at different molecular distributions. Specifically, six different crystal structures of silicon were selected at and between the highest and lowest solid surface molecular densities, while six different amorphous silicon structures were built in the similar surface density range. Wetting angles measured on these surfaces using cylindrical water nano-droplets purged from line tension effects. Wetting angles showed dependence on atomic orientations; contact angles showed up to 38% variation by the change of surface type. More important than the observed angle variation, the aim was to determine the molecules responsible for the variation in wetting. We resolved the solid domains by fine bin-wise molecular densities measured parallel to the surface. Using this data, average near interface solid densities were calculated for each case at different extends from the surface defined by the interface region height parameter. Next, we tried to determine the solid density calculated at which extent can be correlated

better with the observed wetting variation. For each interface extent, we plotted the wetting angles as a function of the corresponding interface solid density. We observed that interface density averaged inside a region of three and more molecular diameter ($h \geq 0.39$ nm) away from the surface cannot describe wetting variation at all. On the other hand, the density of solid region extending 0.13 and 0.26 nm reflects solid structure dependent variation of wetting angle better while this variation is very similar for both single crystalline and amorphous silicon surfaces. Results will be a good contribution to existing theoretical attempts to predict contact angles as a function of interface densities.

Acknowledgements

Authors also would like to thank the Center for Scientific Computation at Southern Methodist University.

Disclosure statement

No potential conflict of interest was reported by the authors.

Funding

This work was supported by the Scientific and Technological Research Council of Turkey (TÜBİTAK) [grant number 217M460] and by the Turkish Academy of Sciences (TUBA) in the framework of the Young Scientist Award Programme (GEBIP).

ORCID


Murat Barisik http://orcid.org/0000-0002-2413-1991

References

[1] Rafiee J, Mi X, Gullapalli H, et al. Wetting transparency of graphene. Nat Mater. 2012;11:217–222. doi:10.1038/nmat3228.
[2] Pham AT, Barisik M, Kim BH. Interfacial thermal resistance between the graphene-coated copper and liquid water. Int J Heat Mass Transf. 2016;97:422–431. doi: 10.1016/j.ijheatmasstransfer.2016.02.040.
[3] Shih CJ, Wang QH, Lin S, et al. Breakdown in the wetting transparency of graphene. Phys Rev Lett. 2012;109. doi: 10.1103/PhysRevLett.109.176101.
[4] Annamalai M, Gopinadhan K, Han SA, et al. Surface energy and wettability of van der Waals structures. Nanoscale. 2016;8:5764–5770. doi: 10.1039/c5nr06705g.
[5] Gaur APS, Sahoo S, Ahmadi M, et al. Surface energy engineering for tunable wettability through controlled synthesis of MoS2. Nano Lett. 2014;14:4314–4321. doi: 10.1021/nl501106v.
[6] Chow PK, Singh E, Viana BC, et al. Wetting of mono and few-layered WS2 and MoS2 films supported on Si/SiO2 substrates. ACS Nano. 2015;9:3023–3031.
[7] Zenkin S, Belosludtsev A, Kos Š, et al. Thickness dependent wetting properties and surface free energy of HfO2 thin films. Appl Phys Lett. 2016;108:231602. doi: 10.1063/1.4953262.
[8] Chen S, Cheng Y, Zhang G, et al. Anisotropic wetting characteristics of water droplets on phosphorene: roles of layer and defect engineering. J Phys Chem C. 2018;122:4622–4627. doi: 10.1021/acs.jpcc.7b10788.
[9] Ramos-Alvarado B, Kumar S, Peterson GP. On the wettability transparency of graphene-coated silicon surfaces. J Chem Phys. 2016;144:014701. doi: 10.1063/1.4938499.
[10] Ramos-Alvarado B, Kumar S, Peterson GP. Wettability of graphitic-carbon and silicon surfaces: MD modeling and theoretical analysis. J Chem Phys. 2015;143:044703. doi: 10.1063/1.4927083.
[11] Shen P, Fujii H, Matsumoto T, et al. Surface orientation and wetting phenomena in Si/α-alumina system at 1723K. J Am Ceram Soc. 2005;88:912–917. doi: 10.1111/j.1551-2916.2005.00180.x.
[12] Grzelak EM, Shen VK, Errington JR. Molecular simulation study of anisotropic wetting. Langmuir. 2010;26:8274–8281. doi: 10.1021/la9046897.
[13] Ho TA, Papavassiliou DV, Lee LL, et al. Liquid water can slip on a hydrophilic surface. Proc Natl Acad Sci. 2011;108:16170–16175. doi: 10.1073/pnas.1105189108.
[14] Sendner C, Horinek D, Bocquet L, et al. Interfacial water at hydrophobic and hydrophilic surfaces: slip, viscosity, and diffusion. Langmuir. 2009;25:10768–10781. doi: 10.1021/la901314b.
[15] Gonzalez-Valle CU, Kumar S, Ramos-Alvarado B. Investigation on the wetting behavior of 3C-SiC surfaces: theory and modeling. J Phys Chem C. 2018. doi: 10.1021/acs.jpcc.7b12271.
[16] Baski AA, Erwin SC, Whitman LJ. The structure of silicon surfaces from (001) to (111). Surf Sci. 1997;392:69–85. doi: 10.1016/S0039-6028(97)00499-8.
[17] Pei QX, Lu C, Fu MW. The rapid solidification of Ti3Al: a molecular dynamics study. J Phys Condens Matter. 2004;16:4203–4210. doi: 10.1088/0953-8984/16/24/002.
[18] Park KW, Park H, Fleury E. Strain localization in annealed Cu50Zr50 metallic glass. Mater Sci Eng A. 2011;528:5319–5326. doi: 10.1016/j.msea.2011.03.079.
[19] Li PT, Yang YQ, Xia Z, et al. Molecular dynamic simulation of nanocrystal formation and tensile deformation of TiAl alloy. RSC Adv. 2017;7:48315–48323. doi: 10.1039/c7ra10010h.
[20] Ma PW, Liu WC, Woo CH, et al. Large-scale molecular dynamics simulation of magnetic properties of amorphous iron under pressure. J Appl Phys. 2007;101. doi: 10.1063/1.2715753.
[21] Horbach J. Molecular dynamics computer simulation of amorphous silica under high pressure. J Phys Condens Matter. 2008.
[22] Peralta J, Gutiérrez G. Pressure-induced structural transition in amorphous GeO2: a molecular dynamics simulation. Eur Phys J B. 2014;87; doi: 10.1140/epjb/e2014-50176-3.
[23] Nguyen GT, Nguyen TT, Nguyen TT, et al. Molecular dynamics simulations of pressure-induced structural and mechanical property changes in amorphous Al2O3. J Non Cryst Solids. 2016;449:100–106. doi: 10.1016/j.jnoncrysol.2016.07.018.
[24] Pompe T, Herminghaus S. Three-phase contact line energetics from nanoscale liquid surface topographies. Phys Rev Lett. 2000. doi: 10.1103/PhysRevLett.85.1930.
[25] Bruot N, Caupin F. Curvature dependence of the liquid-vapor surface tension beyond the Tolman approximation. Phys Rev Lett. 2016. doi: 10.1103/PhysRevLett.116.056102.
[26] Schimmele L, Naplórkowski M, Dietrich S. Conceptual aspects of line tensions. J Chem Phys. 2007. doi: 10.1063/1.2799990.
[27] Malijevsk A, Jackson G. A perspective on the interfacial properties of nanoscopic liquid drops. J Phys Condens Matter. 2012.
[28] Schrader M, Virnau P, Binder K. Simulation of vapor-liquid coexistence in finite volumes: a method to compute the surface free energy of droplets. Phys Rev E – Stat Nonlinear Soft Matter Phys. 2009. doi: 10.1103/PhysRevE.79.061104.
[29] Wilhelmsen Ø, Bedeaux D, Reguera D. Tolman length and rigidity constants of the Lennard-Jones fluid. J Chem Phys. 2015. doi: 10.1063/1.4907588.
[30] Wang JY, Betelu S, Law BM (2001) Line tension approaching a first-order wetting transition: experimental results from contact angle measurements. Phys Rev E. doi: 10.1103/physreve.63.031601
[31] Tolman RC. The effect of droplet size on surface tension. J Chem Phys. 1949. doi: 10.1063/1.1747247.
[32] Kanduč M. Going beyond the standard line tension: size-dependent contact angles of water nanodroplets. J Chem Phys. 2017. doi: 10.1063/1.4990741.
[33] Zhang J, Wang P, Borg MK, et al. A critical assessment of the line tension determined by the modified Young's equation. Phys Fluids. 2018b. doi: 10.1063/1.5040574.

[34] Peng H, Birkett GR, Nguyen AV. The impact of line tension on the contact angle of nanodroplets. Mol Simul. 2014. doi: 10.1080/08927022.2013.828210.
[35] Isaiev M, Burian S, Bulavin L, et al. Efficient tuning of potential parameters for liquid–solid interactions. Mol Simul. 2016;42:910–915. doi: 10.1080/08927022.2015.1105372.
[36] Azouzi MEM, Ramboz C, Lenain JF, et al. A coherent picture of water at extreme negative pressure. Nat Phys. 2013. doi: 10.1038/nphys2475.
[37] Joswiak MN, Duff N, Doherty MF, et al. Size-dependent surface free energy and Tolman-corrected droplet nucleation of TIP4P/2005 water. J Phys Chem Lett. 2013. doi: 10.1021/jz402226p.
[38] Nguyen CT, Barisik M, Kim B. Wetting of chemically heterogeneous striped surfaces: molecular dynamics simulations. AIP Adv. 2018. doi: 10.1063/1.5031133.
[39] Spori DM, Drobek T, Zürcher S, et al. Beyond the lotus effect: roughness influences on wetting over a wide surface-energy range. Langmuir. 2008. doi: 10.1021/la800215r.
[40] De Gennes PG. Wetting: statics and dynamics. Rev Mod Phys. 1985. doi: 10.1103/RevModPhys.57.827.
[41] Zhang H, Chen S, Guo Z, et al. Contact line pinning effects influence determination of the line tension of droplets adsorbed on substrates. J Phys Chem C. 2018a. doi: 10.1021/acs.jpcc.8b03588.
[42] Plimpton S. Fast parallel algorithms for short-range molecular dynamics. J Comput Phys. 1995;117:1–19. doi: 10.1006/jcph.1995.1039.
[43] Ramos-Alvarado B, Kumar S. Spectral analysis of the heat flow across crystalline and amorphous Si-water interfaces. J Phys Chem C. 2017;121:11380–11389. doi: 10.1021/acs.jpcc.7b01689.
[44] Tersoff J. New empirical approach for the structure and energy of covalent systems. Phys Rev B. 1988;37:6991–7000. doi: 10.1103/PhysRevB.37.6991.
[45] Ishimaru M, Munetoh S, Motooka T. Generation of amorphous silicon structures by rapid quenching: a molecular-dynamics study. Phys Rev B. 1997;56:15133–15138. doi: 10.1103/PhysRevB.56.15133.
[46] Ishimaru M. Molecular-dynamics study on atomistic structures of amorphous silicon. J Phys Condens Matter. 2001;13:4181–4189. doi: 10.1088/0953-8984/13/19/301.
[47] Talati M, Albaret T, Tanguy A. Atomistic simulations of elastic and plastic properties in amorphous silicon. EPL. 2009;86:6600. doi: 10.1209/0295-5075/86/66005.
[48] Iordanov TD, Schenter GK, Garrett BC. Sensitivity analysis of thermodynamic properties of liquid water: a general approach to improve empirical potentials. J Phys Chem A. 2006;110:762–771. doi: 10.1021/jp0538868.
[49] Miyamoto S, Kollman PA. Settle: an analytical version of the SHAKE and RATTLE algorithm for rigid water models. J Comput Chem. 1992;13:952–962. doi: 10.1002/jcc.540130805.
[50] Barisik M, Beskok A. Wetting characterisation of silicon (1,0,0) surface. Mol Simul. 2013;39:700–709. doi:10.1080/08927022.2012.758854.
[51] Barisik M, Beskok A. Equilibrium molecular dynamics studies on nanoscale-confined fluids. Microfluid Nanofluidics. 2011;11(3):269–282.
[52] Ingebrigtsen T, Toxvaerd S. Contact angles of Lennard-Jones liquids and droplets on planar surfaces. J Phys Chem C. 2007;111:8518–8523. doi: 10.1021/jp0676235.
[53] Fujii K, Waseda A, Kuramoto N. Development of a silicon density standard and precision density measurements of solid materials by hydrostatic weighing. Meas Sci Technol. 2001. doi: 10.1088/0957-0233/12/12/302.
[54] Kluge MD, Ray JR, Rahman A. Amorphous-silicon formation by rapid quenching: a molecular-dynamics study. Phys Rev B. 1987;36:4234. doi:10.1103/PhysRevB.36.4234.